Structural and Dielectric Properties of Quartz–Water Interfaces

ARTICLE *in* THE JOURNAL OF PHYSICAL CHEMISTRY C · DECEMBER 2008

Impact Factor: 4.77 · DOI: 10.1021/jp803642c

2 AUTHORS, INCLUDING:

Aurora E Clark
Washington State University
80 PUBLICATIONS **1,293** CITATIONS

SEE PROFILE

Structural and Dielectric Properties of Quartz−Water Interfaces

Matthew C. F. Wander and Aurora E. Clark*

Department of Chemistry, Washington State University, Pullman, Washington 99164

Received: April 25, 2008; Revised Manuscript Received: October 19, 2008

The structure, orientation, and dielectric of water at the quartz|water interface has been examined under different hydration levels using classical molecular dynamics. The properties of $1H_2O/10$ Å^2, $2H_2O/10$ Å^2, $4H_2O/10$ Å^2, and bulk water on quartz have been benchmarked against experimental data. Structurally, the simulations match existing sum-frequency spectroscopy data, which indicate the existence and orientation of both frozen and loosely bound water on the quartz surface. Good agreement has also been found with existing experimental dielectric data for the $1H_2O/10$ Å^2 level of hydration, and a clear difference has been found in the values of $\varepsilon_s = 48$, $\varepsilon^{\parallel} = 48$, and $\varepsilon^{\perp} = 40$ for the first slice of a bulk-water−solid interface and $\varepsilon_s = 30$, $\varepsilon^{\parallel} = 30$, and $\varepsilon^{\perp} = 10$ for that of $1H_2O/10$ Å^2 water coverage. Overall there is a fundamental difference in shielding between a single interface and the $1H_2O/10$ Å^2 level of hydration.

Introduction

In this work, the origins of the structured water|quartz interface are examined, and comparisons are made between the bulk water interface and $1H_2O/10$ Å^2 coverage, which is the number of water molecules that exactly covers the quartz surface in a single layer with no excess (based upon the radius of H_2O). Such comparisons are essential because many interfacial properties can be measured only at small hydration levels and extrapolations between the physical properties of bulk and minimal water coverage are uncertain at best.[1−6] Within ab initio studies, the effect of the dielectric constant of water near a surface has largely been ignored. Prior work as focused upon either modeling adsorption structures in a vacuum or invoking a minimal number of explicitly described surface-sorbed waters.[7,8] Yet water plays a dual role in solvation. On one hand, water can play a direct role through ligation or hydrogen bonding where it influences the structural environment, and on the other hand, it can provide charge screening in the form of the dielectric. Explicit water will certainly do the first, but it has been shown that the addition of a dielectric on top of one to two solvation shells provides significant additional benefit.[9] Higher numbers of explicit solvation shells on a quartz surface, to our knowledge, have not been examined using ab initio methods. Experimentally, models have been developed that treat the interface in terms of layers. The double-layer models divide the interface into structured and diffuse layers, though different numbers of structured layers may exist and the diffuse layer is absent in some versions.[10−12] Within the double-layer paradigm, two chemical models have been posed regarding the controlling factors of water interfacial structure. From the theory of 19th century electrodics, the first model places an emphasis upon the bulk physical interface of two different dielectric materials. Here, the difference in the dielectric constants of the solid and the liquid determine the thickness of the structured layer of the liquid interface and its capacitance.[13,14] More recent modifications of this model have incorporated the effects of ion size and charge through parametrization, making it amenable to wide use by experimentalists.[13−16] In practice, the dielectric constant is treated as a fittable experimental parameter regardless of whether the controlling factor for organization is the dielectric of the solid or the choice of ion in the interface. The second chemical model is an outcome of the extensive classical dynamics studies of the solid|water interface. These have demonstrated remarkable consistency with structured water extending one to three layers and a total interface with the diffuse layer on the order of 20 Å.[17−21] From these studies, two factors have emerged as the primary controls of water interlayer structure.[17−21] The first, and presumably most important, is H bonding between the water and the surface. The second is the arrangement of charges within the surface itself.

Commensurate with structural ordering of the water|quartz interface is the inherent change in the physical properties of the structured water. The dielectric constant, ε, can be thought of as a ratio of charge screening of a substance in bulk relative to that of vacuum. In dipolar liquids such as water, the Kirkwood fluctuation formula is often used to calculate the isotropic dielectric constant (ε_s).[22,23]

$$\frac{(\varepsilon_s - 1)(2\varepsilon_s + 1)}{9\varepsilon_s} = y_D G_k(R_{ij}) = y_D \frac{1}{N_0 {\mu_0}^2} \left\langle \sum_{i=1}^{N} \sum_{j=1}^{N} \vec{\mu}_i \cdot \vec{\mu}_j \right\rangle \quad (1)$$

The constant y_D is equal to $4\pi\rho\mu^2/9k_BT$ (4.347 for water at 298.15 K in cgs units), ρ is the number of dipoles per unit volume, k is the Boltzman constant, T is temperature in Kelvin, α^2 is the norm of the dipole of water squared [$(0.41)(e/3.33564 \times 10^{-20})^2$ D^2], N_0 is the number of molecules in the system, μ_i and μ_j are the dipole vectors of molecules i and j, and ε_s is the dielectric constant or permittivity. Equation 1 assumes that the energy of an induced electric field caused either by an interface or some other form, which the water molecules are trying to attenuate, is approximately the same as the energy required to rotate an individual water molecule.[22,23] The Kirkwood model is a refinement of the earlier Onsager model that did not assume correlation between individual water dipoles.[24] Treating water as a point dipole, this formula implies that for Kirkwood liquids the primary contribution to the dielectric constant is the dipole−dipole interaction and that a simple classical description of water is both accurate and chemically realistic. Indeed,

* Author to whom correspondence should be addressed. E-mail: auclark@wsu.edu.

10.1021/jp803642c CCC: $40.75

classical models have been shown to be effective at matching bulk water dielectric properties.[25,26]

The experimental determination of the dielectric constant can be performed using dielectric spectroscopy, which has been applied to both bulk materials and interfaces.[27−29] In the latter, a bulk measurement is still performed but is decomposed into the interfacial water and solid components. By using the frequency-dependent portions of the dielectric spectra it is possible to determine the quantity of water required to hydrate a hydrophobic molecule. These molecules rotate differently from bulk at specific frequencies of an oscillating field and can be distinguished according to that hindrance. This region of hydrophobic hydration has been determined to correspond to just one layer of solvating water molecules.[28,30]

Because dielectric spectroscopy is a frequency-dependent measurement, an extrapolation of that experiment is required to determine the static dielectric constant. A number of existing measurements for water at various levels of hydration coverage on quartz exist.[31−36] One of the most recent measurements, to be extrapolated to a static value, is that from Sakamoto et al. of $\varepsilon_s = 10$ for $1H_2O/10$ Å^2 coverage, which is consistent with previous studies. This work is particularly appealing for the simulations community because it attempts to reconcile the Kirkwood model with the experimental bulk picture, facilitating direct calculation by simulation, but it is still consistent with all previous measurements.[31] Interestingly, dielectric spectroscopy, thermochemical measurements, IR, sum-frequency generation spectroscopy, and many other experimental measurements have found the first adsorbed layer of water on quartz to be "frozen".[31,37−40] This structural immobility is sometimes used to justify the low measured dielectric constant for low water coverage levels and its extrapolation to the structured region of the bulk water interface.[41−44] However, the dielectric constant for highly structured ice is 96, which is higher than for even bulk water.[45] This well-known phenomenon is indicative of the disorder of the protons present in ice (I_h crystal), highlighting that immobility itself is not a good barometer of dielectric behavior.[46−49] Theoretical calculations of the interfacial water dielectric have focused on the effect of fields on the interfacial region and have treated the interface as one unit rather than allowing different regions of the interface (i.e., structured, diffuse, and bulk layers) to have different dielectric screening values.[50,51] In these studies, it has been shown that the primary variations in the isometric dielectric constant result from changes in the z-direction component of ε, indicating that any study that purports to show trends in this behavior needs to account for anisotropy appropriately.

In this study, we use classical mechanics of adsorbed and bulk water on a quartz surface to examine the similarity between the $1H_2O/10$ Å^2, $2H_2O/10$ Å^2, and $4H_2O/10$ Å^2 levels of hydration, with the first structured layer of the bulk-water|quartz interface. The simulation results are then compared to experiment, where the consistency of both computed and experimental structural and dielectric information is demonstrated. We will also compare the MD results to periodic DFT results of the minimum stable configuration of $1H_2O/10$ Å^2 on a unit cell. This will give qualitative insight into the role of temperature in this level of hydration. We hypothesize that there is a fundamental difference in the dielectric screening of a water monolayer and the first structured layer of a bulk interface on the same mineral.

Methods

DFT Calculations. Periodic boundary DFT calculations were performed using Gaussian 03 vB.05 to optimize the geometry and analyze the electronic structure of both quartz and $1H_2O/10$ Å^2 water coverage on quartz.[52] The B3LYP combination of exchange and correlation functionals was used with the lanl2 effective core potential on Si and the lanl2DZ basis on all atoms.[53−56] This basis contains [2s 2p] contracted Gaussian functions on both O and Si, with the inner 10 electrons of Si contained within the effective core potential. The H-atom basis consists of [2s] functions. Although this basis set is too small for accurate energies from cluster calculations, we are focused primarily upon the geometric properties that should be reasonably approximated given the computational requirements for ab initio periodic boundary conditions. The quartz slab had a thickness of a single SiO_2 unit with hydroxyl termination above and below.[57,58]

Molecular Dynamics Simulation Cell. The construction of the simulation cell was performed in Cerius2, starting with a single hexagonal unit cell of quartz whose cell vectors were converted to a rectangular cell for easy analysis.[59] Unit cell conversion was performed by doubling the unit cell volume and altering $\vec{b}$ as follows:

$$\vec{b}_{new} = 2\vec{b}_{old} + \vec{a}_{old} \quad (2)$$

This yielded a rectangular unit cell with dimensions of 4.91 × 8.50 × 5.402 Å^3. A surface was cut in the 001 plane with a slab thickness of 10 unit cells or approximately 60 Å. The two surface Si−O groups on each side of the slab were protonated. A large cell of 5 × 3 cells was combined to form a surface of 24.550 × 25.513 Å^2 on a side. The vacuum gap of ∼60 Å was filled with 1152 water molecules. These were from a pre-equilibrated water box of comparable dimensions. The final length after pressure equilibration is 118 Å (Figure 1). Additional slabs corresponding to $1H_2O/10$ Å^2, $2H_2O/10$ Å^2, and $4H_2O/10$ Å^2 of coverage were created by deleting water molecules from the bulk water slab. The $1H_2O/10$ Å^2 level of hydration was chosen because it is the number of water molecules that exactly covers the quartz mineral surface in a single layer with no excess (due to the density of >Si−O−H groups on the surface). Note that this level of coverage is not necessarily synonymous with a monolayer of water coverage because of the distribution of water configurations at the quartz surface. The final water molecule counts were 28, 55, and 118 molecules for the $1H_2O/10$ Å^2, $2H_2O/10$ Å^2, and $4H_2O/10$ Å^2 hydration layers, respectively.

Molecular Dynamics Methods. After an initial Cerius2 minimization of 500 steps, classical molecular dynamics (MD) simulations were performed using the program LAMMPS[60,61] and the CLAYFF force field. For complete details on the CLAYFF force field, see Cygan et al.[62] CLAYFF uses a flexible SPC water model.[63−65] We used CLAYFF partial charges for all atoms in our simulation slab. In the case of water, the charges are −0.82 for the oxygen and +0.41 for the hydrogen atoms. This model gives a dielectric of 84, which is slightly higher than the experimental value of 78.[26] A nearly identical cousin of this model SCP/E has been known to give excellent results for interfaces and under high electric field values.[19,51]

LAMMPS calculations were performed on the surface slabs. The time step for all MD simulations was 1 fs. First, a 100 ps equilibration NVE (NVE: constant number, volume, and energy) MD simulation was performed, and then a 500 ps NPT (NPT: constant number, pressure, and temperature) simulation was performed at ∼1 bar ($P = 0$ GPa) and 300 K. In the latter

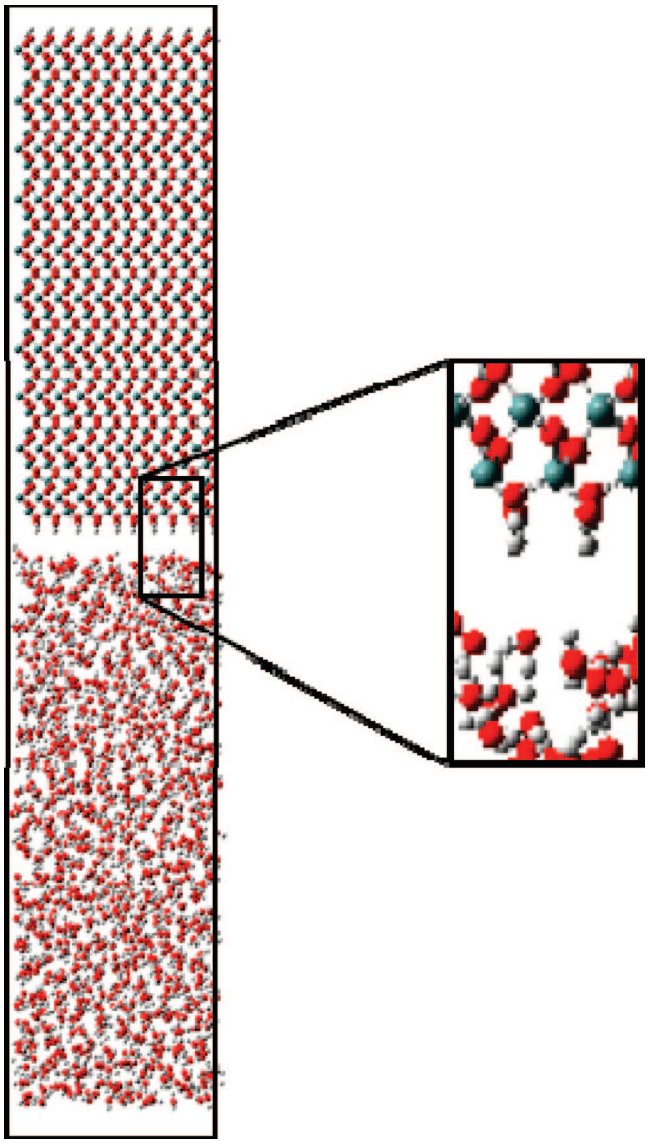

Figure 1. (001) quartz slab and water simulation box, with an inset showing the arrangement of the unit cell.

simulation, only the z direction of the simulation cell was allowed to vary. This allowed the water in the simulation cell to reach a density appropriate to the surface conditions. For the $1H_2O/10$ Å^2, $2H_2O/10$ Å^2, and $4H_2O/10$ Å^2 hydration layer simulations, NVE was substituted for NPT. The final z dimension for all of the slabs was 118 Å. Dipole orientation and other position data were sampled for each quartz−water system in a subsequent simulation that ran for 1 ns using an NVT ensemble ($T = 300$ K). Long-range sums were computed using the Ewald method as implemented in LAMMPS. Cartesian coordinates for all atoms were tabulated at every time step.

Two Fortran codes were used to analyze the trajectory files from the MD simulations. The first code, written by Andre Kalinichev, was used to determine the vertical atomic density profile, cross-sectional surface maps for the atoms, and average dipole vectors for the water molecules.[66] The second code, written for this publication, sorts the water molecules according to their orientation into H-up (z_{H1} and $z_{H2} > z_O$), H-down (z_{H1} and $z_{H2} < z_O$), and H-side ($z_{H1} < z_O < z_{H2}$ or $z_{H2} < z_O < z_{H1}$), where z is the distance in the z direction from the slab surface (Scheme 1). It then performs the same set of analyses on the oriented waters as the Kalinichev script.

SCHEME 1: Pictoral Representation of Water Orientation[a]

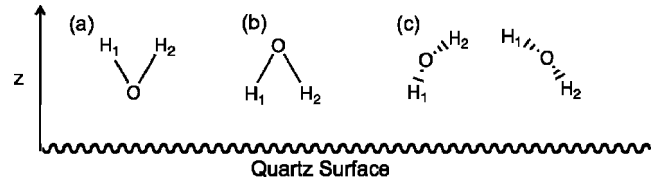

[a] (a) H-up, (b) H-down, and (c) H-side.

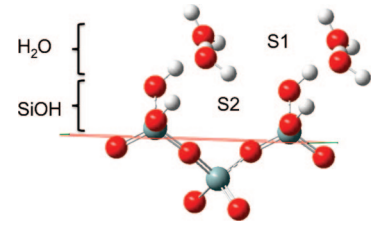

Figure 2. B3LYP/lanl2DZ-optimized hydrated SiO_2 with a monolayer of water. The primary adsorption site (S1) and a potential secondary adsorption site (S2) are highlighted. All four waters shown here are in site S1.

Calculation of the Dielectric Constant. The truncated Kirkwood method, as implemented by Richardi, was used to calculate the dielectric constant of water in the interfacial region.[67] The original form of the fluctuation formula for calculating a dielectric constant is derived via the Kirkwood constant, G_k. This constant that has been shown to determine the dielectric of a dipolar medium, such as liquid water, is a function of the dipole of each individual molecule and its interaction with all of its nearest neighbors.[22,68] We can simplify eq 1 for water as follows because $\varepsilon_s \gg 1$:

$$y_D G_k = (2\varepsilon_s - 1)/9 \tag{3}$$

To further save on computational time, we can utilize the fact that correlation declines to zero after two solvation shells, and thus the fluctuation formula can be truncated radially:[67]

$$G_k(R_{ij}) = \frac{1}{N_0 {\mu_0}^2}\left\langle \sum_{i=1}^{N}\sum_{j=1}^{N} \vec{\mu}_i \cdot \vec{\mu}_j \right\rangle, \; R_{ij} < R_{\text{trunk}} \tag{4}$$

where R_{ij} is the distance between the i and j water molecules. R_{trunk} is typically defined as the first maximum in the Kirkwood function or 6 Å, which for a simple ion or individual water molecule corresponds to two solvation shells, after which bulk behavior is expected. There are dielectric effects from the surface that extend well beyond 6 Å. This is an important confirmation that the truncation is not obscuring long-range effects of the surface on water orientation and rotation.

Using the isotropic dielectric constant, it is possible to calculate a dielectric tensor. The dielectric tensor, a diagonal 3 × 3 matrix, incorporates the effects of the dielectric interface on image dipoles and other local field distortions in the vicinity of the interface. Given the symmetry at the interface, $\varepsilon_x = \varepsilon_y$ and may be expressed as $\varepsilon^{\parallel}$, which thus incorporates the influence of G_k[69,70]

$$\varepsilon_s^{\parallel}(z) - \varepsilon_s(\infty) = \frac{\varepsilon_s - 1}{32\pi\varepsilon_0 z^3}\frac{\varepsilon_s - \varepsilon_1}{\varepsilon_s + \varepsilon_1} \times \left[\frac{3\varepsilon_s \beta \mu^2 G_k}{(2\varepsilon_s - 1)^2} - 4\pi\varepsilon_0 {R_{\text{wat}}}^3 \frac{\varepsilon_s - 1}{2\varepsilon_s + 1}\right] \tag{5}$$

where $\varepsilon_s(\infty) = \varepsilon_s$, the bulk or isotropic dielectric constant, ε_1 is the bulk dielectric constant of the material forming the interface

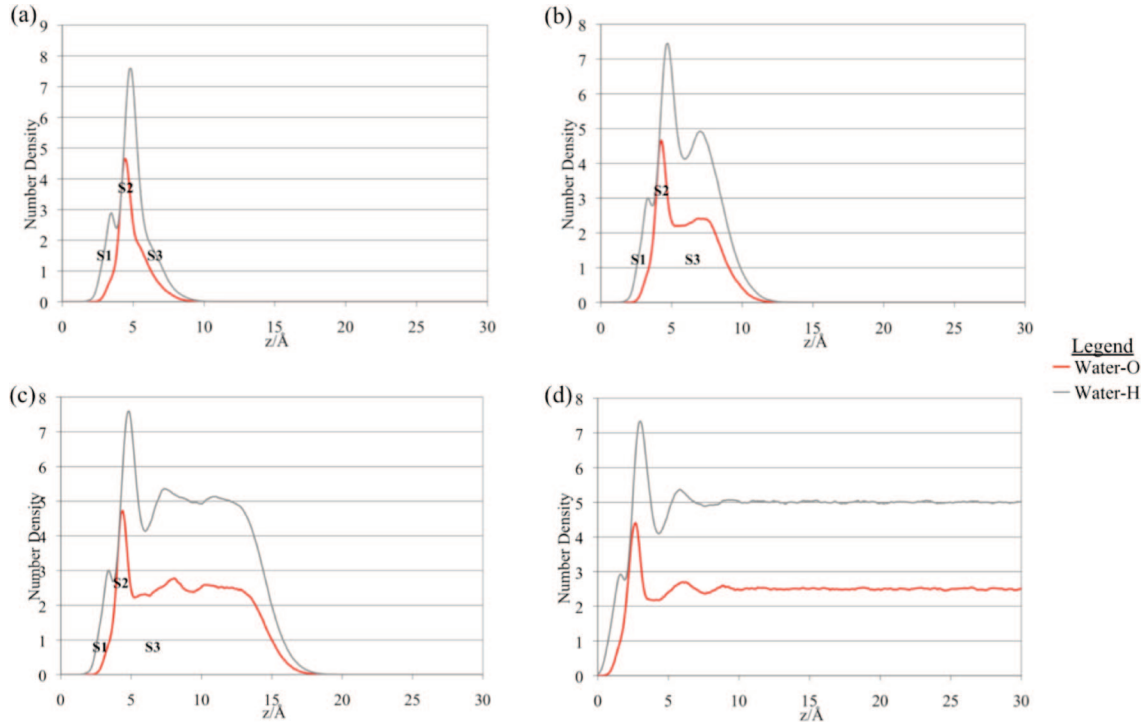

Figure 3. MD vertical water profiles for water|quartz interfaces: (a) $1H_2O/10$ Å^2, (b) $2H_2O/10$ Å^2, (c) $4H_2O/10$ Å^2, and (d) bulk water.

($\varepsilon_{1(\text{quartz})} = 2$), ε_0 is the permittivity of vacuum, z is the distance of the water dipole from the interface, β is $1/k_BT$, μ is the dipole moment of one water molecule, G_k is the Kirkwood correlation factor, and R is the radius of one water molecule determined from ρ, the number density. We assume that $z \geq R_{\text{wat}}$. Individual water molecules do not penetrate the interface. As presented by Finken in eq 16 of ref 70, the expression for $\varepsilon^{\perp}$ is valid only for $z \gg R$. Therefore, we utilize the general relationship between $\varepsilon^{\parallel}$ and $\varepsilon^{\perp}$

$$\varepsilon_s^{\perp}(z) = \frac{\varepsilon_s}{1 + 2(\varepsilon_s^{\parallel}(z) - \varepsilon_s(\infty))} \tag{6}$$

where all of the above components have the same meaning as in eq 5. This expression is easily derived from eqs 7 and 12a/b in ref 70.

Given the magnitudes of $\varepsilon^{\parallel}$ and $\varepsilon^{\perp}$, the relative error in the calculation becomes significant. All errors were calculated using a time-averaged standard deviation of the entire simulation. It was also assumed that because the sampling was every time step we were slightly oversampling our data because it takes about 10 steps to complete a H−O stretch. This worked out to an error in our calculated constants of ∼5−10%. This happens to be approximately the same error associated with the Kirkwood truncation. For the tensor, the dependence of these expressions on the fluctuation correlation term (G_k) is the same as in the isometric case, so we presumed that the error would be similar to G_k, which is the primary source of error in our calculations.

Results and Discussion

The structural and electrochemical aspects of the interfaces for bulk water|quartz and 1, 2, and $4H_2O/10$ Å^2 coverage were first examined. The nonbulk simulations are considered to have water hydration layers that are double interfaces with water sandwiched between the quartz and vacuum. Taken as a sequence, they illustrate a process of hydration from monolayer to full saturation. At each level of hydration, a consistent set of analyses were performed to elucidate the physical and structural properties of water. Vertical number density profiles, water orientation vertical density profiles, z-dipole projections, and dielectric tensor calculations were performed. For the $1H_2O/10$ Å^2 level of coverage and the bulk, we also determined and analyzed the surface maps of the oriented waters. We assumed that the $1H_2O/10$ Å^2 and bulk surface maps would provide good end-member cases of the horizontal adsorption behavior and that the $2H_2O/10$ Å^2 and $4H_2O/10$ Å^2 levels of hydration would be representative of transitions in between the two systems. The combination of these analyses allows a complete vertical and horizontal profile of the water structure, which was then compared with known surface adsorption sites.

Water Structure. The DFT-optimized geometry (Figure 2) of a single water per 10 Å^2 on quartz shows a static picture of a low-energy water arrangement wherein both waters are hydrogen bonded to a primary adsorption site. Indeed, one water molecule prefers binding at what is labeled the primary site (S1). However, a second accessible site (S2 in Figure 2) is indicated by the fact that one of the waters is a H-bond donor to a >SiOH group. Although the DFT structure will not be the same as for the dynamics results, it can be used to determine the effects of temperature on the real monolayer structure.

The vertical distribution function (VDF) within the dynamics simulation of one monolayer (Figure 3a) shows a primary peak with two distinct shoulders corresponding to two different adsorption sites. The primary peak corresponds to the S1 site observed in the DFT-optimized structure (Figure 2) where the water receives a H bond from the >SiOH groups on the surface. Unlike the DFT structure, the dynamic picture has only partial occupation of the primary site. The first shoulder in Figure 3a corresponds to waters that are sandwiched in between two SiOH groups (site S2 in Figure 2). The second shoulder corresponds to waters that have coalesced on the surface to form a droplet of water that corresponds to the second layer of adsorption (labeled S3). Whereas differences between the hydrogen and the oxygen profiles might imply that the first shoulder represents waters

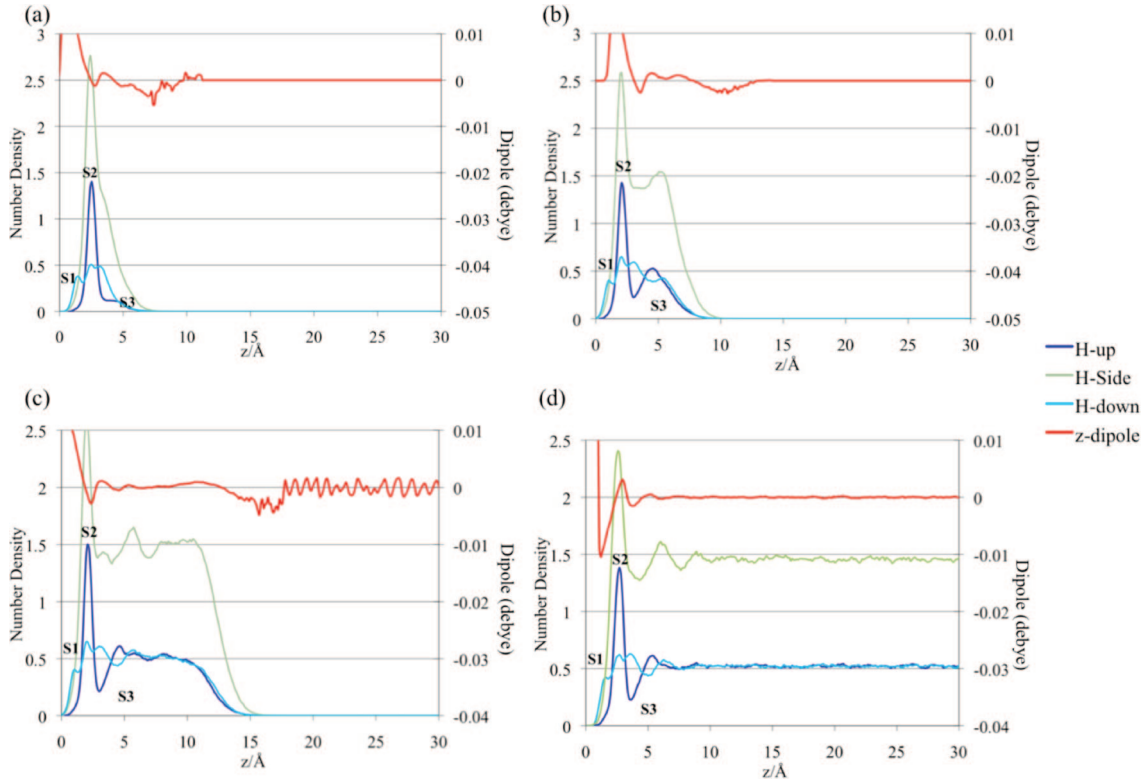

Figure 4. MD water orientation profiles (O-atom number density) of the water|quartz interface: (a) $1H_2O/10$ Å^2, (b) $2H_2O/10$ Å^2, (c) $4H_2O/10$ Å^2, and (d) bulk water. Note that the side waters will outnumber the up or down by 2:1:1 and that this is an even distribution of water due to the method of counting.

with their hydrogens pointed toward the surface and the second shoulder represents waters with their hydrogens pointing away from the surface, this feature can be addressed conclusively only by mapping the water orientations, shown subsequently.

Generally, the VDF of the $2H_2O/10$ Å^2 level of coverage is similar to the $1H_2O/10$ Å^2 case (Figure 3b). The same three adsorption sites are observed in both the $1H_2O/10$ Å^2 and $2H_2O/10$ Å^2 saturation levels, though the population of the S3 site has increased in occupancy.

In the $4H_2O/10$ Å^2 case (Figure 3c), adsorption at the primary and secondary sites is nearly identical to that in the $2H_2O/10$ Å^2 simulation. Indeed, all of the additional water has gone into the second hydration layer (bilayer), which is characterized by site S3.

The VDF of bulk water (Figure 3d) has two primary peaks before the number density converges to its bulk value. Site S3, which corresponds to the third peak/shoulder in the $1H_2O/10$ Å^2 level of saturation, corresponds in the bulk VDF to the flat region following the first two peaks. The first two peaks indicate a structured water layer thickness of about 8 Å, though the nature of MD averaging means that the second layer may not be that rigid. Otherwise, a clear connection to the less saturated systems is observed. In particular, the leading shoulder site is present, and in the bulk simulation, there is an indication of a second rise found in the density in the $4H_2O/10$ Å^2 structure.

Water Orientation. The water orientation profiles shown in Figure 4 give substantially more information as to the nature of the three water adsorption sites present in $1H_2O/10$ Å^2 through $4H_2O/10$ Å^2 levels of coverage. Coupled with the information about the *z*-dipole projections, the water orientation can be elucidated because of the complimentary nature of the two orientation approaches. Whereas the discussion here concerns all of the graphs in Figure 4, it is assumed that the $1H_2O/10$ Å^2 basic structure underlies all of the adsorption arrangements.

Secondary Adsorption Site, S2. The waters in this adsorption site, which appear as the first shoulder in the orientation profiles in all simulations, are clearly pointing down. This site is labeled in Figure 2 as S2 and can now be clarified as a bridging adsorption site with the two water hydrogens donating H-bonds to the surface SiOH groups. This site is likely to be higher in energy than S1 but is clearly thermally accessible.

Primary Adsorption Site, S1. This site is shown as the second peak in all simulations and is a mixture of H-up waters and H-side waters. H bonding and local dipole influences from the surface drive the former. This site is labeled in Figure 2 as S1. The latter orientation is driven by the need to form a stable H-bond network within the water layer and potentially by some influence from the vacuum interface above it.

Third Adsorption Site, S3. Represented by the third peak in the graphs in Figure 4, site S3 is almost exclusively driven by side-oriented waters because of the need to form a stable H-bond network in response to the vacuum interface. This adsorption site is not labeled in Figure 2 because it does not necessarily have a fixed position relative to the surface. Beyond the $1H_2O/10$ Å^2 level of hydration, as site S3 accumulates it exhibits oscillatory transitory behavior to the bulk, which may mitigate the possibility of long-range dipolar forces. These oscillations extend out approximately 8−10 Å corresponding to the limits of the structured region of the interface.

Relation to Experiment. Three adsorption sites and three possible orientations of water have been identified on the quartz surface. Of the sites, the first two (S1 and S2) are inner sphere and the third (S3) is outer sphere. Inner sphere indicates that the water is directly H bonded to the surface whereas outer sphere means that its adsorption is connected to the surface through another water molecule. Although all three orientations have some small probability of existing in each site, a single orientation appears to define the physical character of the site.

TABLE 1: Quartz Monolayer through Tetralayer Dielectric Values, Calculated by MD Simulation as a Bulk Value, with the Isometric Dielectric, ε_s, Parallel Component, $\varepsilon^{\parallel}$, and Perpendicular Component, $\varepsilon^{\perp}$, of the Dielectric Presented

surface coverage	$\varepsilon_s/\varepsilon^{\parallel}$	$\varepsilon^{\perp}$
1.0/Å^2	34.1 ± 1.5/32.7 ± 1.5	9.6 ± 1.5
2.0/Å^2	38.3 ± 3.4/38.2 ± 3.4	29.8 ± 3.4
4.0/Å^2	46.5 ± 4.0/46.4 ± 4.0	40.8 ± 4.0

TABLE 2: 2 H_2O/Å^2 Water|Quartz Vertical Dielectric Profile, as Calculated by MD Simulation, with the Isometric Dielectric, ε_s, Parallel Component, $\varepsilon^{\parallel}$, and Perpendicular Component, $\varepsilon^{\perp}$, of the Dielectric Presented[a]

	z = 0.0−2.8 Å	z = 2.8−3.8 Å	z = 3.8−10.4 Å
$\varepsilon_s/\varepsilon^{\parallel}$	15.5/13.6 ± 1.1	145.1/144.3 ± 7.5	22.0/19.1 ± 2.0
$\varepsilon^{\perp}$	3.20 ± 1.1	56.3 ± 7.5	3.2 ± 2.0

[a] The differences in the $\varepsilon^{\perp}$ values from Table 1 illustrate the significance of the z value in the Finken expressions.

TABLE 3: 4 H_2O/Å^2 Water|Quartz Tetralayer Vertical Dielectric Profile, As Calculated by MD Simulation, with the Isometric Dielectric, ε_s, Parallel Component, $\varepsilon^{\parallel}$, and Perpendicular Component, $\varepsilon^{\perp}$, of the Dielectric Presented[a]

	z = 0.0−2.8 Å	z = 2.8−4.4 Å	z = 4.4−7.3 Å	z = 7.3−16.0 Å
$\varepsilon_s/\varepsilon^{\parallel}$	31.0/29.6 ± 2.6	128.8/128.4 ± 6.0	78.9/78.7 ± 12.9	27.4/26.2 ± 10.1
$\varepsilon^{\perp}$	8.2 ± 2.6	76.1 ± 6.0	59.1 ± 12.9	8.0 ± 10.1

[a] The differences in the $\varepsilon^{\perp}$ values from Table 1 illustrate the significance of the z value in the Finken expressions.

The first adsorption site (S2) between the >SiOH groups is characterized by inner-sphere adsorption of H-down waters, whereas the second site (S1) is characterized by inner-sphere adsorption of O-down waters. The outer-sphere adsorption site (S3) is characterized by H-side water. Using sum-frequency generation (SFG) spectroscopy, the water structure at a quartz surface has been characterized by the degree of mobility at thermal energies, labeled "frozen" and "loose".[38] The first category is further divided into two orientations: H-down and O-down. Loose water is characterized by having an H-down orientation.[38] Experimentally, Sakamoto has also characterized the first 1H_2O/10 Å^2 of adsorbed water on quartz as frozen, suggesting that direct inner-sphere adsorption inhibits water mobility.[31] A qualitative similarity is observed between the first two adsorption sites in our model of the H-down and O-down subcategories of experimentally observed and structurally immobile water adsorbed on a quartz surface. As in the experimental water|quartz interfacial studies, approximately half of the simulated frozen water is O-down (S1) and half is H-down (S2). Finally, a direct comparison can be made between the side-oriented outer-sphere adsorption layer (S3) and experiment, provided that H-down in the experimental orientation means one H atom down. In this case, the structural match of our simulation to the structures predicted by the SFG study is essentially the same.

Dielectric Constants. The dielectric constants calculated using eqs 2, 4, and 5 are shown in Tables 1−3 and in Figure 5. As a general observation, only small differences exist between the parallel component of the dielectric, $\varepsilon^{\parallel}$, and the isometric constant, ε_s, but none were significant. The perpendicular component of the dielectric, $\varepsilon^{\perp}$, is significantly lower in the first one to two layers from the interface. Overall, a clear contrast is observed between the water in the 1H_2O/10 Å^2 hydration level and the first structured layer in the bulk-water|quartz interface,

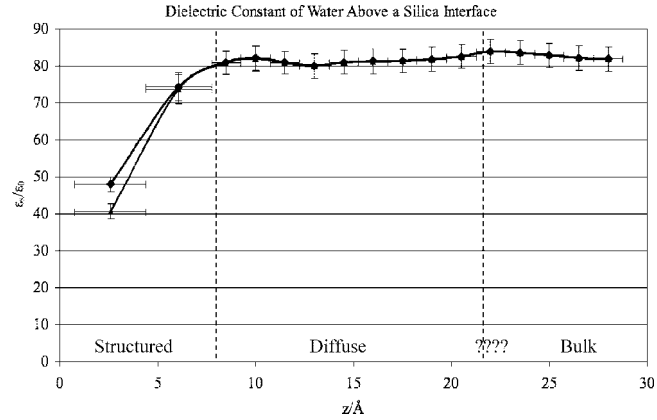

Figure 5. MD dielectric profile for the bulk-water|quartz interface. Isometric values, ε_s, (diamond) with the perpendicular component, $\varepsilon^{\perp}$, (dot). Approximate transition zones between structured, diffuse, and bulk regions are presented.

TABLE 4: Double-Layer Model (DLM) and Triple-Layer Model (TLM) Capacitances for the Structured Layers of the Bulk-Water|Quartz Interface as Calculated from MD Simulations

slice	distance/Å	average dielectric[a]	capacitance (μF/cm^{-2})
DLM (ε_s)	7.00	60.5 ± 2.2	76.6 ± 2.8
DLM ($\varepsilon^{\perp}$)	7.00	56.3 ± 2.2	71.3 ± 2.8
TLM slice 1(ε_s)	3.67	48.0 ± 2.1	115.7 ± 5.0
TLM slice 1($\varepsilon^{\perp}$)	3.67	40.6 ± 2.1	97.9 ± 5.0
TLM slice 2(ε_s)	3.33	74.4 ± 3.9	197.9 ± 10.4
TLM slice 2($\varepsilon^{\perp}$)	3.33	73.7 ± 3.9	196.1 ± 10.4

[a] Note that the dielectrics are relative to a bulk value of 84 given by the SPC water model.

and important differences exist in the dielectric screening behavior of each of the systems, shown subsequently (Tables 1−3 and Figure 5).

1H_2O/10 Å^2 Hydration Level. The dielectric for this amount of water saturation is particularly important because it represents the primary experimental evidence for benchmarking our model. Sakamoto et al. measured it to be 10.[31] To incorporate such a low value into a Kirkwood−Onsager-type expression, Sakamoto fitted the dipole moment of an interfacial water molecule at only 1.03 D, an unlikely value to say the least. Given that Sakamoto's value is a bulk measurement, it is reasonable to assume that the measurement is some average of $\varepsilon^{\parallel}$ and $\varepsilon^{\perp}$. The parallel ($\varepsilon^{\parallel}$) and perpendicular ($\varepsilon^{\perp}$) components of the 1H_2O/10 Å^2 dielectric within our simulations are 30 and 10, respectively (Table 1), yet Sakamoto's experimental average should not be confused with the formal isometric value, ε_s. It can be argued that because of refraction any random slice through a quartz grain would preferentially measure the perpendicular component. Given the qualitative nature of the calculation, this is nearly as close to an exact match as is possible to achieve with this approach.

2H_2O/10 Å^2 and 4H_2O/10 Å^2 Hydration Levels. Here a rise is observed in both $\varepsilon^{\parallel}$ and $\varepsilon^{\perp}$ components each time, driven by an internal layer that is further from the interface (Table 1). This rise is very significant for being merely an additional 2 Å away from the interface. It indicates that the transition from the 1H_2O/10 Å^2 level of coverage to the bulk interface occurs rapidly with the addition of small amounts of water, and it helps to explain the clear differences between the bulk water and the monolayer systems.

Bulk Interface. Within the bulk water simulation, the dielectric screening is quite high all the way up the first

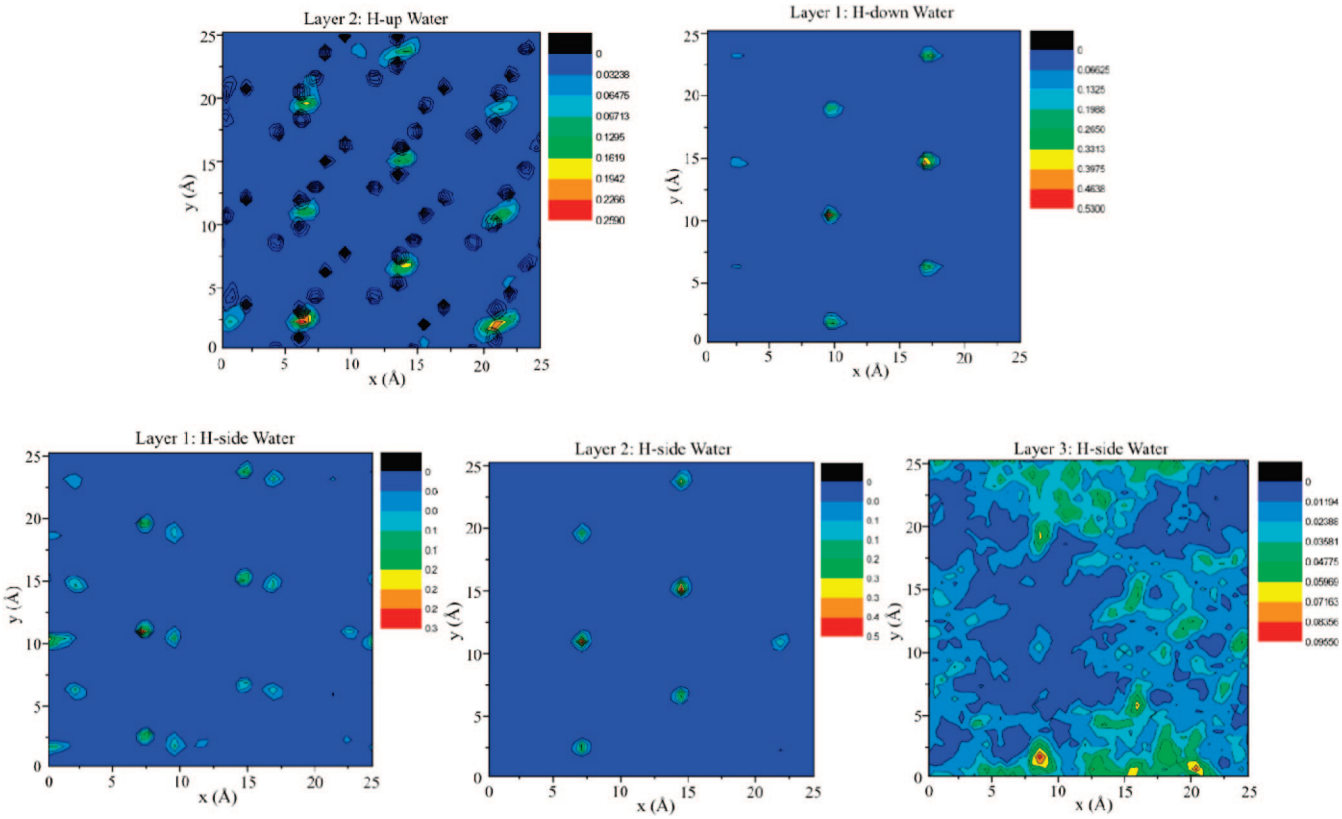

Figure 6. Surface maps of oxygen density for slice 2 of the H-up water molecules, slice 1 of the H-down water molecules, and slices 1−3 of the H-side water molecules in the $1H_2O/10$ Å^2 water:quartz interface. Note slice 2 of the H-up water has a transparent overlay of the H-atom positions. Surface maps for slice 2−3 H-down water molecules and slice 1 and 3 H-up are shown in Supporting Information.

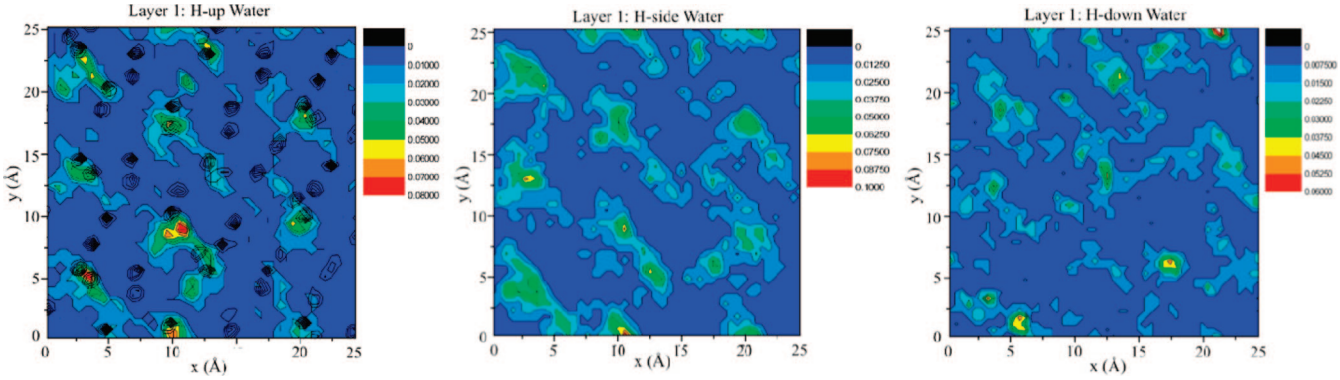

Figure 7. Surface maps of oxygen density for slice 1 of the H-up, H-side, and H-down water molecules in the bulk-water|quartz interface. Note that slice 1 of the H-up water has a transparent overlay of the H-atom positions. Surface maps for slices 2 and 3 are shown in Supporting Information.

structured layer (Table 2). Starting at $\varepsilon \approx 40$ at the interface, it rises rapidly until the value is ∼4 below the bulk value for the diffuse layer. The perpendicular component drops slightly within in the structured region, but only the difference in the first structured layer is significant. This indicates that when quartz is in contact with bulk solution a significant dielectric is available to screen charges approaching the interface, and it is likely that this could have an important effect on surface reactivity.

Capacitances of the Structured Region. In Table 4, the calculated capacitances for the structured region of the bulk-water|quartz interface are presented. Whereas the perpendicular component, $\varepsilon^{\perp}$, is likely to determine the capacitance, the isometric value is shown for comparison. It should be noted that capacitances for $\varepsilon^{\perp}$ and ε_s are not generally statistically distinguishable. The double-layer model (DLM) capacitance is an average over the entire structured layer. The triple-layer model (TLM) capacitances treats the two structured slices separately, so capacitances were determined for each of the two slices separately and are labeled TLM slices 1 and 2 in Table 4.

Surface Maps of Oriented Water. Surface maps were sliced according to changes in the orientation profile. The first slice starts at zero and ends at the crossing point of the H-down and H-up vertical density curves (∼1.9 Å). The second slice ends at the next crossing point in the vertical density profile (∼2.9 Å), and the third slice ends at the point where the total water density goes to zero (∼5.4 Å).

$1H_2O/10$ Å^2 Level of Hydration. Here, an absolute difference between the H-up waters and the H-down waters is observed. In Figure 6, the first two slices of the H-up waters are clearly situated above the SiOH groups, and the H-down waters are situated between them. Because the first two slice distributions

of H-up waters are the same, this indicates that the H-up waters are not actually changing their adsorption site as a function of slice; they are only translating up and down slightly, which is also the case with the H-down waters. The H-side distribution in slice 1 is clearly a mixture of H-up and H-down water sites, whereas the H-side distribution in slice 2 matches only the H-up site. For the third slice, we see some structure, but it is profoundly asymmetric. This is probably a result of clumping and the need to form as complete a H-bonding network as possible.

Bulk Interface. Only the first two slices ($z = 0-2.1$ and 2.1−3.2Å) of each orientation are discussed here because after the second slice there is no structure for any of the orientations (Supporting Information). The first slice for the three orientations (Figure 7) is similar to the $1H_2O/10$ Å^2 case, but the structure is much less defined. For the most part, the H-up-oriented waters are above the SiOH groups, and the H-down are in between, with the H-side being an average of the two. Where structure is present in the second slice, it appears to be a more diffuse representation of that observed in slice 1 (Supporting Information). As in the $1H_2O/10$ Å^2 case, water is able to translate up and down freely between the slices, so changing between H-up and H-down orientations is not likely within a given adsorption site. Given that H-side waters coexists with both H-up and H-down waters, flipping from H-up to H-side and H-down to H-side is also observed.

Transitions between Layers. According to the water orientations, the vertical density profiles, and the dielectric, there is a clear transition between the structured and diffuse layers, but there is only a very limited distinction between the diffuse and bulk layers. Between these two regions, there is only a very slight difference in the isometric dielectric constant of ∼4. Distinctions between the diffuse and bulk regions may become more apparent in situations in which a concentration gradient of ions is present, but that is beyond the scope of this study.

Further Considerations. An important and fundamental contradiction of theory exists in the study of dielectrics and is principally due to its application to bulk properties (fields, permittivity, and screening). Though some models have modifications to incorporate molecular effects as in the Kirkwood fluctuation formula, when these modifications are viewed in the context of an interface their underlying premises become problematic. Sakamoto's experimental approach to treating the water|quartz interface for $1H_2O/10$ Å^2 of hydration coverage was to treat the molecular dipole of water as an adjustable parameter. The reduction in the magnitude of the dipole in order to fit the experimental data can be viewed in the context of the image dipoles causing an apparent decrease in the energy of rotating a dipole in the vicinity of a dielectric interface.[41] Finken's theoretical treatment is fundamentally a hybrid between molecular and bulk scales of behavior. Given Finken's success here for matching Sakamoto's experimental data, the question arises as to what causes dielectric behavior at a molecular level. One assumption of the original Kirkwood formulation may help to bring clarity. This assumption states that the energy of the imposed electric field is not greater than the energy of hindered rotation. When the two energies are considered at the individual molecular level, they are approximately equal. Yet what if the energy required to rotate a water molecule far exceeds the field? What if it is so much higher that the water cannot complete a rotation? In this case, could the quantity of dielectric shielding itself be reduced? In this situation, the reduction of a water molecule's ability to rotate might reduce the quantity of dielectric shielding itself, which ia similar in magnitude to a proportional reduction in the effective dipole. Experimental evidence suggests that this is the case; however, such questions are far from being answered and should be considered in the study of interfacial dielectric properties.[28,30]

Conclusions

Classical simulations have been successful at reproducing the available experimental structural and dielectric behavior of a quartz|water interface. Three distinct adsorption sites have been observed: two frozen or structurally immobile and one loose. These correspond roughly to three different orientations of water: H-down, H-up, and H-side. These simulations predict that the dielectric reduction for the $1H_2O/10$ Å^2 level of water coverage on the surface is a direct result of the double interface of water sandwiched between quartz and vacuum. We must stress, however, that many factors, including a polarizable water molecule model or a different water molecule dipole, could have a significant effect on the results, and future work will examine the influence of these variables upon calculated dielectric properties. In both the $2H_2O/10$ Å^2 and $4H_2O/10$ Å^2 systems, transitional behavior is observed relative to the bulk interface. These results are consistent with the limited dielectric sheath where only one layer of water is significantly perturbed relative to bulk. Such dielectric shielding is likely to play an important role in the surface chemistry of many processes, including adsorption and catalysis.

Acknowledgment. This work was sponsored by the U.S. Department of Energy, Office of Nuclear Energy, Science and Technology, Junior Faculty Award Program award #DE-FG07-05ID14692/IDNE006. This research was performed using the Molecular Science Computing Facility (MSCF) in the William R. Wiley Environmental Molecular Sciences Laboratory, a national scientific user facility sponsored by the U.S. Department of Energy's Office of Biological and Environmental Research and located at the Pacific Northwest National Laboratory, operated for the Department of Energy by Battelle.

Supporting Information Available: A comparison of saturated-water-structured layers versus water monolayer structure on quartz via surface maps of oxygen density. This material is available free of charge via the Internet at http://pubs.acs.org.

References and Notes

(1) Yuan, S. L.; Ma, L. X.; Zhang, X. Q.; Zheng, L. Q. *Colloids Surf., A* **2006**, *289*, 1.
(2) Jug, K.; Nair, N. N.; Bredow, T. *Surf. Sci.* **2005**, *590*, 9.
(3) Wang, J. W.; Kalinichev, A. G.; Kirkpatrick, R. J.; Cygan, R. T. *J. Phys. Chem. B* **2005**, *109*, 15893.
(4) Prelot, B.; Poinsignon, C.; Thomas, F.; Schouller, E.; Villieras, F. *J. Colloid Interface Sci.* **2003**, *257*, 77.
(5) Prelot, B.; Villieras, F.; Pelletier, M.; Razafitianamaharavo, A.; Thomas, F.; Poinsignon, C. *J. Colloid Interface Sci.* **2003**, *264*, 343.
(6) Odelius, M. *Phys. Rev. Lett.* **1999**, *82*, 3919.
(7) Rustad, J. R. Molecular Models of Surface Relaxation, Hydroxylation, and Surface Charging at Oxide-Water Interfaces. In *Molecular Modeling Theory: Applictions in the Geosciences*; Cygan, R. T., Kubicki, J. D., Eds.; Mineralogcal Society of America: Washington, DC, 2001; *Vol. 42*.
(8) Rosso, K. M. Structure and Reactivity of Semiconducting Mineral Surfaces: Convergence of Modeling and Experiment. In *Molecular Modeling Theory: Applictions in the Geosciences*; Cygan, R. T., Kubicki, J. D., Eds.; Mineralogcal Society of America: Washington, DC, 2001; *Vol. 42*.
(9) Uudsemaa, M.; Tamm, T. *J. Phys. Chem. A* **2003**, *107*, 9997.
(10) Stern, O. *Z. Electrochem.* **1924**, *30*, 508.
(11) Yates, D. E.; Levine, S.; Healy, T. W. *J. Chem. Soc., Faraday Trans.s I* **1974**, *70*, 1807.
(12) Davis, J. A.; James, R. O.; Leckie, J. O. *J. Colloid Interface Sci.* **1978**, *63*, 480.

(13) Sverjensky, D. A.; Fukushi, K. *Environ. Sci. Technol.* **2006**, *40*, 263.
(14) Sverjensky, D. A. *Geochim. Cosmochim. Acta* **2001**, *65*, 3543.
(15) Henderson, D.; Gillespie, D.; Nagy, T.; Boda, D. *Mol. Phys.* **2005**, *103*, 2851.
(16) Hayes, K. F.; Redden, G.; Wendell, E.; Leckie, J. O. *J. Colloid Interface Sci.* **1991**, *142*, 448.
(17) Predota, M.; Cummings, P. T.; Wesolowski, D. J. *J. Phys.Chem. C* **2007**, *111*, 3071.
(18) Predota, M.; Vlcek, L. *J. Phys. Chem. B* **2007**, *111*, 1245.
(19) Predota, M.; Bandura, A. V.; Cummings, P. T.; Kubicki, J. D.; Wesolowski, D. J.; Chialvo, A. A.; Machesky, M. L. *J. Phys. Chem. B* **2004**, *108*, 12049.
(20) Predota, M.; Zhang, Z.; Fenter, P.; Wesolowski, D. J.; Cummings, P. T. *J. Phys. Chem.y B* **2004**, *108*, 12061.
(21) Spohr, E. *Electrochim. Acta* **2003**, *49*, 23.
(22) Kirkwood, J. G. *J. Chem. Phys.* **1939**, *7*, 911.
(23) Oster, G.; Kirkwood, J. G. *J. Chem. Phys.* **1943**, *11*, 0175.
(24) Onsager, L. *J. Am. Chem. Soc.* **1936**, *58*, 1486.
(25) Bursulaya, B. D.; Kim, H. J. *J. Chem. Phys.* **1998**, *109*, 4911.
(26) Mizan, T. I.; Savage, P. E.; Ziff, R. M. *J. Phys. Chem.* **1994**, *98*, 13067.
(27) McCafferty, E.; Zettlemoyer, A. C. *Discuss. Faraday Soc.* **1971**, *52*, 239.
(28) Wachter, W.; Buchner, R.; Hefter, G. *J. Phys. Chem. B* **2006**, *110*, 5147.
(29) Miller, J. F.; Velev, O.; Wu, S. C. C.; Ploehn, H. J. *J. Colloid Interface Sci.* **1995**, *174*, 490.
(30) Urry, D. W.; Peng, S.; Xu, J.; McPherson, D. T. *J. Am. Chem. Soc.* **1997**, *119*, 1161.
(31) Sakamoto, T.; Nakamura, H.; Uedaira, H.; Wada, A. *J. Phys. Chem.* **1989**, *93*, 357.
(32) Fiat, D.; Folman, M.; Garabatski, U. *Proc. R. Soc. London, Ser. A* **1961**, *260*, 409.
(33) Molyneux, J. E. *J. Math. Phys.* **1970**, *11*, 1172.
(34) Kamiyoshi, K.; Odake, T. *J. Chem. Phys.* **1953**, 1295.
(35) Thorp, J. T. *J. Phys. Chem.* **1966**, *62*, 1086.
(36) Kourosaki, S. *J. Phys. Chem.* **1954**, *58*, 320.
(37) Bellissent-Funel, M.-C.; Lal, J.; Bosio, L.; Physique, L. *J. Chem. Phys.* **1992**, *98*, 4247.
(38) Li, I.; Bandara, J.; Shultz, M. J. *Langmuir* **2004**, *20*, 10474.
(39) Yang, J.; Wang, E. G. *Curr. Opin. Mater. Science.* **2006**, *10*, 33.
(40) Li, T.-D.; Gao, J.; Szoszkiewicz, R.; Landman, U.; Riedo, E. *Phys. Rev. B* **2007**, *75*, 115415. **2007**, 75, 115415.
(41) Dill, K. A.; Bromberg, S. *Molecular Driving Forces: Statistical Thermodynamics in Chemistry and Biology*; Garland Science: New York, 2003.
(42) Gregory, J. *Particles in Water: Properties and Processes*; IWA Publisher: Boca Raton, FL, 2006.
(43) Bottcher, C. J. F. *Theory of Electric Polarization*; Elsevier: Amsterdam, 1973; Vols. *1 and 2*.
(44) Parks, G. A. Surface Energy and Adsorption at Mineral/Water Interfaces: An Introduction. In *Mineral−Water Interface Geochemistry*; Hochella, M. F., White, A. F., Eds.; Mineral Society of America: Washington, DC, 1990; Vol. 23, pp 133.
(45) Dorsay, N. E. *Properties of Ordinary Water Substances*; Reinhold Publishing: New York, 1940.
(46) Rahman, A.; Stillinger, F. H. *J. Chem. Phys.* **1972**, *57*, 4009.
(47) Rick, S. W.; Haymet, A. D. J. *J. Chem. Phys.* **2003**, *118*, 9291.
(48) Adams, D. J. *J. Phys. C* **1984**, *17*, 4063.
(49) Batista, E. R. X., S. S.; Jonnson, H. *J. Chem. Phys.* **1999**, *111*, 6011.
(50) Ballenegger, V.; Hansen, J.-P. *J. Chem. Phys.* **2005**, *122*, 114711.
(51) Yeh, I.-C.; Berkowitz, M. L. *J. Chem. Phys.* **1999**, *110*, 7935.
(52) Frisch, M. J.; Trucks, G. W.; Schlegel, H. B.; Scuseria, G. E.; Robb, M. A.; Cheeseman, J. R.; Montgomery, J. A., Jr.; Vreven, T.; Kudin, K. N.; Burant, J. C.; Millam, J. M.; Iyengar, S. S.; Tomasi, J.; Barone, V.; Mennucci, B.; Cossi, M.; Scalmani, G.; Rega, N.; Petersson, G. A.; Nakatsuji, H.; Hada, M.; Ehara, M.; Toyota, K.; Fukuda, R.; Hasegawa, J.; Ishida, M.; Nakajima, T.; Honda, Y.; Kitao, O.; Nakai, H.; Klene, M.; Li, X.; Knox, J. E.; Hratchian, H. P.; Cross, J. B.; Bakken, V.; Adamo, C.; Jaramillo, J.; Gomperts, R.; Stratmann, R. E.; Yazyev, O.; Austin, A. J.; Cammi, R.; Pomelli, C.; Ochterski, J. W.; Ayala, P. Y.; Morokuma, K.; Voth, G. A.; Salvador, P.; Dannenberg, J. J.; Zakrzewski, V. G.; Dapprich, S.; Daniels, A. D.; Strain, M. C.; Farkas, O.; Malick, D. K.; Rabuck, A. D.; Raghavachari, K.; Foresman, J. B.; Ortiz, J. V.; Cui, Q.; Baboul, A. G.; Clifford, S.; Cioslowski, J.; Stefanov, B. B.; Liu, G.; Liashenko, A.; Piskorz, P.; Komaromi, I.; Martin, R. L.; Fox, D. J.; Keith, T.; Al-Laham, M. A.; Peng, C. Y.; Nanayakkara, A.; Challacombe, M.; Gill, P. M. W.; Johnson, B.; Chen, W.; Wong, M. W.; Gonzalez, C.; Pople, J. A. *Gaussian 03, revision C.02*; Gaussian, Inc.: Wallingford, CT, 2004.
(53) Becke, A. D. *J. Chem. Phys.* **1993**, *98*, 5648.
(54) Stephens, P. J.; Devlin, F. J.; Chabalowski, C. F.; Frish, M. J. *J. Phys. Chem.* **1994**, *98*, 11623.
(55) Hay, A. S. *J. Polym. Sci., Part A: Polym. Chem.* **1998**, *36*, 505.
(56) Dunning, T. H.; Hay, P. J. In *Methods of Electronic Structure Theory*; Schaefer, H. F., III. Plenum Press: New York, 1977; *Vol. 2*.
(57) Clark, A. E.; Sonnennberg, J.; Hay, P. J.; Martin, R. L. *J. Chem. Phys.* **2004**, *121*, 2563.
(58) Maseras, F.; Morokuma, K. *Chem. Phys. Lett.* **1992**, *195*, 500.
(59) *Cerius2, version 4*; Accelerys Software Inc.: 2005.
(60) Plimpton, J.; Pollock, R.; Stevens, M. Proceedings of the Eighth SIAM Conference on Parallel Processing for Scientific Computing, Minneapolis, MN, 1997.
(61) Plimpton, S. J. *J. Comput. Phys.* **1995**, *117*, 1.
(62) Cygan, R. T.; Liang, J.-J.; Kalinichev, A. G. *J. Phys. Chem. B* **2004**, *108*, 1255.
(63) Berendsen, H. J. C.; Postma, J. P. M.; van Gunsteren, W. F.; Hermans, J. Interaction Models for Water in Relation to Protein Hydration. In *Intermolecular Forces*; Pullman, B., Ed.; Kluwer: Boston, 1981.
(64) Reidel, D.; Teleman, O.; Jonsson, B.; Engstrom, S. *Mol. Phys.* **1987**, *60*, 193.
(65) Wallqvist, A.; Teleman, O. *Mol. Phys.* **1991**, *74*, 515.
(66) Kalinichev, A. Personal communication.
(67) Richardi, J.; Fries, P. H.; Millot, C. *J. Mol. Liq.* **2005**, *117*, 3.
(68) Frohlich, H. *Theory of Dielectrics: Dielectric Constant and Dielectric Loss*; Clarendon Press: Oxford, U.K., 1949.
(69) Finken, R. Personal communication.
(70) Finken, R.; Ballenegger, V.; Hansen, J.-P. *Mol. Phys.* **2003**, *101*, 2559.

JP803642C